Non-locality of the contact line in dynamic wetting phenomena

Non-locality of the contact line in dynamic wetting phenomena

Alex V. Lukyanov*

School of Mathematical and Physical Sciences, University of Reading, Reading RG6 6AX, UK

E-mail: a.lukyanov@reading.ac.uk

Abstract

Hypothesis: The notion of the contact line is fundamental to capillary science, where in a large category of wetting phenomena, it was always regarded as a one-dimensional object involving only microscopic length scales. This prevailing opinion had a strong impact and repercussions on the developing theories and methodologies used to interpret experimental data. It is hypothesised that this is not the case under certain conditions leading to non-local effects and requiring the development of a modified force balance at the contact line.

Theory and simulations: Using the first principles of molecular dynamic simulations and a unique combination of steady state conditions and observables, the microscopic structure of the contact region and its connections with macroscopic quantities of capillary flows was revealed for the first time.

Findings: The contact line is shown to become a non-local, macroscopic object involving rather complex interplay between microscopic distributions of density, velocity and friction force. It was established that the non-locality effects, which cannot be in principle captured by localised methodologies, kick off at a universal tipping point and lead to a modified force balance. The developed framework is applicable to a wide range of capillary flows to identify and analyse this regime in applications.

Keywords: *dynamic wetting, nano-scale, meso-scale, contact line, molecular dynamics simulations.*

Introduction

In 1805, Thomas Young proposed an equation to predict the value of the equilibrium contact angle formed by the free surface of a liquid on a solid substrate.[1,2] The Young's equation, in the case of a partially wetting liquid, states that

$$\gamma_{GS} - \gamma_{LS} = \gamma \cos\theta_0, \qquad (1)$$

where θ_0 is the equilibrium contact angle, γ_{GS}, γ_{LS} and γ are gas-solid, liquid-solid and liquid-gas equilibrium interfacial tensions respectively. Equation (1) represents a balance of all surface tension forces acting on the contact line in the tangential to the substrate direction. At the same time, it is also a manifestation of the contact line microscopic dimensions, implying that the contact line can be regarded as a one-dimensional, string-like object in the macroscopic description.

The Young's equation has been revisited and debated many times in the past,[3–6] but ultimately verified down to nanoscale in static conditions.[7] Also, it has been shown recently that this equation, in a slightly modified form, works well in dynamic situations of advancing contact line motion.[8] In this case, the modified Young's law

$$\gamma \cos\theta_0 = \gamma_{GS} - \gamma_{LS} = F + \gamma \cos\theta_c \qquad (2)$$

relates dynamic contact angle θ_c with an extra friction force F acting on the moving contact line. In static conditions, the friction force vanishes and the contact angle should attain the equilibrium value in the absence of the hysteresis effects.

In both static and dynamic scenarios recreated in molecular dynamics simulations (MDS), the local character of the contact line was directly established.[7,8] It has been found that the contact line region, where the non-hydrodynamic force F in the modified Young's law (2) was generated, was on the microscopic length scale of a few atomic distances, as it has been first postulated in the molecular kinetic theory.[8–11]

As it appears, the locality of the contact line region has played an important role in the modelling methodologies of the dynamic wetting phenomena. In the current study, we consider a situation, where the local character of the contact line region is completely broken.

In general, non-locality in dynamic wetting is usually expected in the presence of surface tension gradients (Marangoni effect) created by gradients of temperature or relative concentrations of surface phase components so that macroscopic, large scale hydrodynamic motion can influence the local contact angle.[12] The contact angle can be also influenced directly if the system length scale is comparable to that of the contact line region, in particular at the nanoflow conditions.[13,14]

The situation, we are about to study here, does not fit any of those scenarios. It is fundamentally different and more general in a sense. Indeed, in simple liquids at constant temperature, the interfaces are supposed to be at equilibrium without any gradients of surface tensions.[15,16] So that, if the system size is macroscopic, one may expect that the contact line dynamics will be local and follow the modified Young's equation (2).

But, in a fairly common situation, when the contact line evolution is accompanied by the presence of a precursor film, one may expect that even for simple fluids and large systems in the absence of temperature gradients, the wetting dynamics would be essentially non-local.

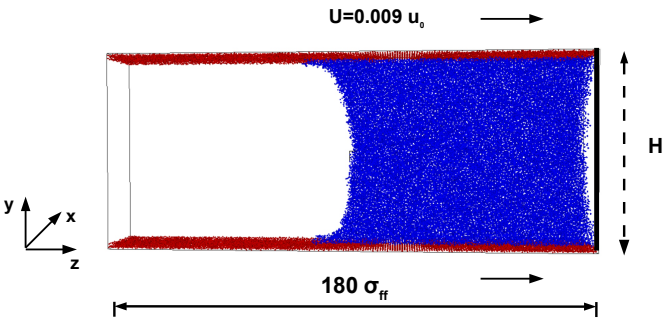

Figure 1: Snapshot of the MDS cylindrical droplet set-up in steady state at $\theta_c = 68.7 \pm 1^\circ$ with the solid wall moving along the z-direction at $U = 0.009\, u_0$. The set-up is periodic in the x-direction with the total number of liquid particles in the simulations varied between $90,000$ to $140,000$.

One may seek to answer the following questions. Would the concept of the moving contact line be only applicable to the tip of the moving precursor film or to a much larger region? How can the contact angle be defined in this case and how would it be influenced in the presence of the film by microscopic distributions?

Previously, we have analysed the dynamic wetting phenomena in the case of advancing motion in the absence of a precursor film focusing on the mechanisms of the force generating the dynamic contact angle and the macroscopic boundary conditions to the governing equations of fluid mechanics.[8,17] Here, the analysis is concentrated on the force balance, in particular in the presence of a precursor, and on the behaviour of the contact angle and the effects of non-locality at the contact line region.

We first briefly formulate the MDS setup and then consider the onset of the precursor films to bridge with the existing theories and experimental observations. Then, we turn our attention to the microscopic structure of the contact line zone and its interconnections with the dynamic contact angle contrasting two cases: with and without a precursor film present.

Conceptually, we will introduce the conflux

region corresponding to the geometric intersection of the two interfacial layers at the contact line zone, at the solid substrate and of the free surface. This will help to define and analyse the effects of non-locality serving as a guidance in contrasting the cases with and without a precursor present.

Initially, the effects of non-locality and the force balance will be illustrated in nano-scale systems in the absence of a precursor, when non-hydrodynamic forces of comparable magnitude to the capillary force strength appear due to the action of the friction force at the contact line on a length scale larger than that of the conflux region.

At the same time, we will demonstrate that in this case the non-locality effects disappear in the macroscopic limit, when the length scale of the friction force tends to the interfacial length scale of the size of the conflux region. So that the force balance is given by (2), where the force F is only due to the friction force distribution, which is completely in the conflux region.

The onset of a precursor, as we will further demonstrate, marks a dramatic change of the size of the contact line region and, as a consequence, the force balance, leading to non-local effects insensitive to the system size. In the end, we will compare the theoretical results with some experimental observations of drops spreading.

Setup and simulations

To study dynamic wetting at the onset of the precursor film regime, we make use of large scale MDS with particles interacting via the Lennard-Jones (LJ) potentials. The details of the methodology of simulations and evaluation of the system parameters, such as the contact angle, can be found in[8,17] and in the Supplementary Material. The geometry of MDS is periodic in the x-direction with reflective boundary conditions at the simulation box ends in the z-direction, Fig. 1. The size of the system in the z-direction was set to prevent any influence of the reflective potential on the liquid particles at the tip of the precursor film.

All units in the model are non-dimensional, such that m_f, σ_{ff}, ε_{ff} and $\tau_0 = \sigma_{ff}\sqrt{\frac{m_f}{\varepsilon_{ff}}}$ provide basic scales for mass, length, energy and time respectively. Here, ε_{kl} and σ_{kl} are the characteristic energy and length scale of LJ interactions, and m_k is the mass of the interacting particles, where one distinguishes between two kinds of particles: liquid (index $k, l = f$) particles of mass m_f and solid wall (index $k, l = w$) particles of mass $m_w = 10\, m_f$. The derived quantities, σ_{ff}^{-3}, $u_0 = \sqrt{\varepsilon_{ff} m_f^{-1}}$, $f_0 = \varepsilon_{ff}\sigma_{ff}^{-3}$, $\gamma_0 = \varepsilon_{ff}\sigma_{ff}^{-2}$ and $\mu_0 = \sqrt{\varepsilon_{ff} m_f}\sigma_{ff}^{-2}$ provide necessary scales for particle density, velocity, pressure, surface tension and viscosity.

The size of the system in the y-direction, height H was set to $H = 63\,\sigma_{ff}$ to have sufficiently small aspect ratio of the interfacial width ($h_s \approx 4\,\sigma_{ff}$ to $8\,\sigma_{ff}$) to the size of the bulk region. Test runs with $H = 102\,\sigma_{ff}$ have shown no effects on the bulk region of this parameter.

The layer thickness in the periodic x-direction (droplet depth) was set at $\Delta x = 18\,\sigma_{ff}$ for the simulations with short chain molecules $N_B = 5$ and at $\Delta x = 29\,\sigma_{ff}$ for simulations involving longer chains. A test run with a larger depth $\Delta x = 50\,\sigma_{ff}$ at $N_B = 50$ has shown no influence of this parameter on the macroscopic observables. The results have been averaged over the droplet depth, that is in the x-directions with no, on average, any structure observed over the droplet depth. The cylindrical geometry of the droplet has also helped to avoid any line tension effects, which may become influential at the nanoscale.

To mimic the forced wetting regime, the solid wall particles were moving with velocity U in the z-direction ([1,0,0] crystallographic direction), where the reflective wall was acting as a piston at rest. After initial equilibration during $\Delta t_{eq} = 10000\,\tau_0$ with the time integration step $\Delta t_s = 0.01\,\tau_0$, which was used in the study, we reached a steady state and measured dynamic contact angle and other interfacial parameters. We note that the essential part of the current methodology was based on the ability to reach a steady state to obtain good signal-to-noise ratio results. In contrast to the previous studies,

where the onset of a precursor was observed,[18] the steady state conditions allowed to exclude other factors, such as the constantly evolving droplet shape, which may influence the dynamics of both the precursor film and the contact line region, where the contact angle is defined, inflate the parameter space and obscure the effects of dynamics wetting.

It should be noted that the hysteresis effects of different physical origin associated with surface inhomogeneities either present (surface roughness or varying chemical composition) or induced (due to the surface deformations and the finite time of the accommodation of the substrate) are beyond the scope of this study.[19–25] The hysteresis effects are expected to become important in the case of inhomogeneous and/or soft surface compositions, such as polymer brushes for example. The solid substrate in the MDS was set to be atomically rough only, that is sufficient to create a friction force, but otherwise homogeneous, and quite rigid, details can be found in the Supplementary Material. So that the surface deformations were negligible and the relaxation time in the solid was found to be short, on the time scale of ballistic motion of the substrate particles, comparable to the relaxation time found in the liquids.[15,16]

Consider now how the precursors appear in the MDS setup.

The onset of the precursor film regime

Precursor films of different dimensions varied between macroscopic, mesoscopic (a few tens of nanometers) and microscopic (molecularly thin films) length scales have been regularly observed experimentally and in MDS.[26–38]

The wetting front of a molecularly thin film, emanating at the foot of the liquid volume, was found propagating according to a diffusion law,

$$L_p = \sqrt{D_s t}, \tag{3}$$

similar to the Lucas-Washburn kinetics.[26–28,30,38] Here L_p is the length of the pre-

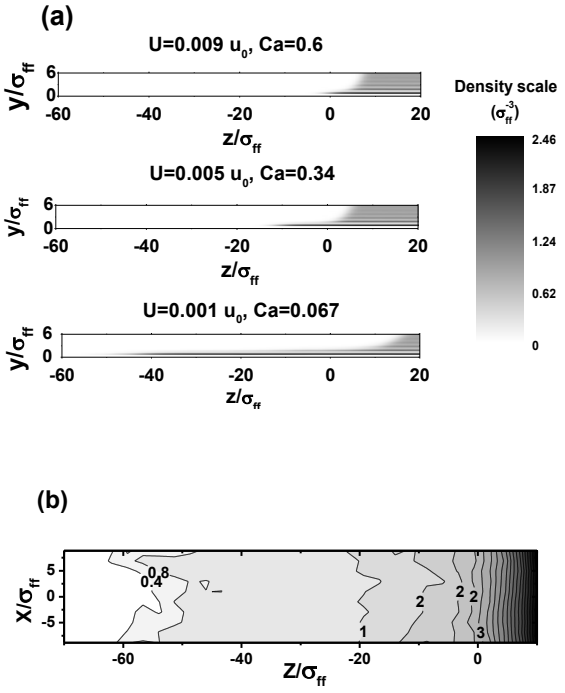

Figure 2: Illustration of the onset and development of the precursor film in a steady state in MDS. (a) Particle density at different velocities U (capillary numbers $Ca = \mu U/\gamma$) at $N_B = 50$, $T_0 = 1\,\epsilon_{ff}/k_B$ and $\epsilon_{wf} = 1.3\,\epsilon_{ff}$ (b) Integrated particle density $\rho_b^{-1}\int \rho\, dy$ at $N_B = 5$, $T_0 = 0.8\,\epsilon_{ff}/k_B$, $\epsilon_{wf} = 1.2\,\epsilon_{ff}$ and $U = 0.001 u_0$. Distance y is measured from the equimolar surface of the solid wall particles, distances x and z are measured from the centre of the simulation box.

cursor film counted from the foot of the macroscopic region and D_s is the effective coefficient of surface diffusion.

From (3), the velocity of the moving film front

$$\frac{dz_f}{dt} = \frac{1}{2}\sqrt{\frac{D_s}{t}} = \frac{D_s}{2L_p} \tag{4}$$

vanishes with time and with the film length.

This observation implies that for a moving droplet (the foot is moving) the film length should attain a constant value

$$L_p = \frac{D_s}{2U} \tag{5}$$

when

$$\frac{dz_f}{dt} = U. \tag{6}$$

In the MDS, the precursor film was only observed in the complete wetting cases ($\theta_0 = 0$), when the droplet velocity was below some critical value $U < U_T$, Tables 1 and 2. The case of ultra small contact angles may require a special study.

The typical steady state of the precursor film observed in the MDS for liquids consisting of short ($N_B = 5$) and long ($N_B = 50$) chain molecules is illustrated in Fig. 2. As one can see, the film structure is homogeneous, the thickness $h_f = \rho_b^{-1} \int \rho \, dy$ varies from $h_f \approx 1\,\sigma_{ff}$ at the tip of the film to $h_f \approx 2\,\sigma_{ff}$ closer to the foot of the bulk volume at $z = 0$. The variations across the film (in the x-direction) are not very strong demonstrating thermally induced fluctuations of the tip position Fig. 2.

We consider now the steady state in detail and compare with the previous studies.

Results and discussion

To understand the basic properties of the precursor film, consider first how our MDS results correspond to the predictions of the previously developed diffusion theory represented by equation (3), which was also found to comply with experimental observations.

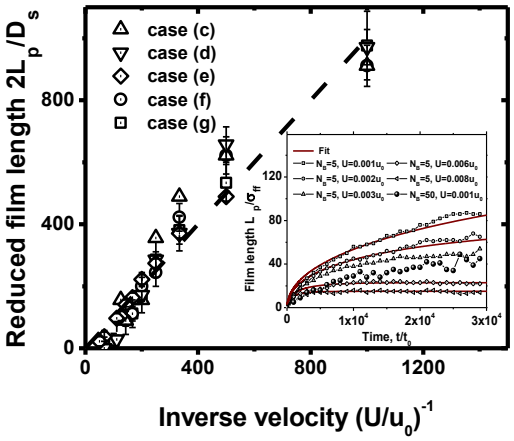

Figure 3: Reduced precursor film length $2L_p/D_s$ as a function of the inverse reduced droplet velocity u_0/U in the steady state at different system parameters T, N_B and ε_{wf}. Parameter u_0 is the MDS velocity scale. The dashed line is the fit $L_p = D_s/2U$. Inset illustrates the precursor film dynamics while the MDS system was reaching the steady state. Precursor film length L_p as a function of time t at different contact line velocities U and molecular length N_B at $T = 1\varepsilon_{ff}/k_B$ and $\varepsilon_{wf} = 1.4\,\varepsilon_{ff}$. The solid lines are the fits given by (8).

Evolution and the steady state of the precursor film

Integrating the evolution equation

$$\frac{dL_p}{dt} = \frac{D_s}{2L_p} - U, \quad L_p \in \left(0, \frac{D_s}{2U}\right) \tag{7}$$

with the initial condition $L_p(0) = 0$, one gets

$$t = \frac{L_p}{U} - \frac{D_s}{2U^2} \ln\left(1 - \frac{2UL_p}{D_s}\right). \tag{8}$$

To verify the evolution law (8) obtained from (3) at $U < U_T$, MDS were initiated from a steady state attained at a velocity above the critical value $U > U_T$, when no precursor film was initially present.

The precursor film evolution at different conditions was monitored using integrated density profiles, Fig. 3 (inset), where the front position was ascribed to the point where $\int_0^\infty \rho \, dy = 0.9\,\sigma_{ff}^{-2}$.

The film length has indeed attained a con-

Table 1: Parameters of the MDS systems and dynamic wetting regimes: N_B is the number of beads in the molecules, k_BT is the temperature of the liquid (k_B is the Boltzmann constant), ρ_b is the bulk liquid particle density, μ is the zero shear rate liquid viscosity, γ is the surface tension of the liquid at the free surface, ε_{wf} is the liquid-solid particle LJ interaction energy, Π_s is the particle density of the substrate, γ_{SL} is the surface tension of the liquid at the solid, γ_{GS} is the surface tension of the gas at the solid, θ_0 is the static contact angle, and F_c and U_c are the characteristic force per unit length and the characteristic velocity used to generate the master curve in Fig 4. Parameters μ_0, γ_0 and u_0 are used to obtain reduced quantities in MDS, see Supplemental Material for details.

Set	N_B	k_BT/ε_{ff}	$\rho_b\sigma_{ff}^3$	μ/μ_0	γ/γ_0	$\varepsilon_{wf}/\varepsilon_{ff}$	$\Pi_s\sigma_{ff}^3$	γ_{SL}/γ_0	γ_{GS}/γ_0	θ_0 (deg)	F_c/γ_0	U_c/u_0
(a)	5	0.8	0.91	10.5	0.92	0.9	4	-0.66	0	44	1.57	0.03
(b)	15	1	0.88	18	0.83	0.8	4	-0.21	0	75	1.03	0.042
(c)	5	0.8	0.91	10.5	0.92	1.2	1.4	-2.3	0	0	3	0.025
(d)	5	0.8	0.91	10.5	0.92	1.4	1.4	-3.48	0	0	3.96	0.011
(e)	5	1	0.86	5.7	0.71	1.4	1.4	-1.62	0	0	1.31	0.0049
(f)	50	1	0.89	61.8	0.92	1.3	1.4	-2.2	0	0	2.73	0.0074
(g)	50	1	0.89	61.8	0.92	1.4	1.4	-2.6	0	0	2.86	0.0033

Table 2: Parameters of the MDS systems and the precursor films in the full wetting regimes: N_B is the number of beads in the molecules, k_BT is the temperature of the liquid (k_B is the Boltzmann constant), μ is the zero shear rate liquid viscosity, γ is the surface tension of the liquid at the free surface, ε_{wf} is the liquid-solid particle LJ interaction energy, γ_{SL} is the surface tension of the liquid at the solid, D_s is the effective coefficient of surface diffusion obtained by fitting velocity dependencies $L_p(U)$ in the steady state, Fig. 3, h_f is the average film thickness in the steady state and F_T and U_T are the values of the force per unit length and velocity at the transition point into the wetting regime with the precursor film present. Parameters μ_0, u_0 and γ_0 are used to obtain reduced quantities in MDS, see Supplemental Material for details.

Set	N_B	k_BT/ε_{ff}	μ/μ_0	γ/γ_0	$\varepsilon_{wf}/\varepsilon_{ff}$	γ_{SL}/γ_0	$D_s/\sigma_{ff}\sqrt{\frac{\varepsilon_{ff}}{m_f}}$	h_f/σ_{ff}	U_T/u_0	F_T/F_c	U_T/U_c
(c)	5	0.8	10.5	0.92	1.2	-2.3	0.09 ± 0.01	2.1	0.04	0.83	1.6
(d)	5	0.8	10.5	0.92	1.4	-3.48	0.07 ± 0.01	2.1	0.017	0.81	1.55
(e)	5	1	5.7	0.71	1.4	-1.62	0.27 ± 0.04	2	0.008	0.85	1.63
(f)	50	1	61.8	0.92	1.3	-2.2	0.09 ± 0.01	1.1	0.012	0.81	1.62
(g)	50	1	61.8	0.92	1.4	-2.6	0.084 ± 0.01	1.1	0.005	0.84	1.52

stant value over time with (8) providing a good approximation to the resulting film dynamics with only one parameter D_s in (8) being varied in the fitting. The observable steady state length matches closely that by (5), Fig. 3. This allows to independently determine diffusion coefficient D_s, Table 2, which was found to be consistent with the values required to fit temporal dependencies in Fig. 3 (inset). Indeed, at $N_B = 5$, $\varepsilon_{wf} = 1.4\,\varepsilon_{ff}$ and $T = 1\,\epsilon_{ff}/k_B$, $D_s = 0.27 \pm 0.04\,\sigma_{ff}\sqrt{\frac{\varepsilon_{ff}}{m_f}}$, while in fitting the curves in Fig. 3 (inset) it was $D_s = 0.3 \pm 0.06\,\sigma_{ff}\sqrt{\frac{\varepsilon_{ff}}{m_f}}$.

The obtained values of D_s are in line with the estimate from the analysis in hydrodynamic approximation $D_s \approx \frac{2h_fS_0}{3\mu}$ (S_0 is the initial spreading parameter) despite the microscopic character of the precursor film.[27] In the same conditions, using $h_f = 2 \pm 0.2\,\sigma_{ff}$ and the bulk viscosity μ, $D_s = 0.21 \pm 0.02\,\sigma_{ff}\sqrt{\frac{\varepsilon_{ff}}{m_f}}$.

Parametrically, an increase in the solid wall potential ε_{wf} (away from the wetting transition) and in the chain length N_B would reduce the ability of molecules to diffuse along the substrate and hence shall lead to a reduced coefficient of diffusion D_s.[35] On the other hand, an

increase in the liquid temperature is expected to produce an opposite effect. All those trends have been clearly observed in the MDS, Table 2. As it was noticed previously, the bulk viscosity of long chain molecules does not proportionally contribute into the liquid mobility, that is the bulk and the surface viscosity may differ, see, for example, cases (e) and (g).[18,33,38]

One can conclude here that, the dynamics and the steady state of the precursor film correspond well to that expected according to the linear diffusion model, when the liquid motion in the film is initiated by the force generated at the tip of the film, while the energy is dissipated through the friction at the substrate.

Consider now the behaviour of macroscopic observables, namely the dynamic contact angle, where several new effects have been observed.

The onset of the precursor film and dynamic contact angle

The transition to the wetting regime with the precursor film present can be clearly observed in the dependence of the out-of-balance contact line force

$$F = \gamma(\cos\theta_0 - \cos\theta_c) \tag{9}$$

as a function of the reduced droplet velocity U/U_c, Fig. 4, where parameters F_c and U_c were chosen to bring the dependencies into a master curve, Table 1.

In the case of complete wetting, the out of balance force can be formally calculated on the basis of the equilibrium surface tensions

$$F = \gamma_{GS} - \gamma_{LS} - \gamma\cos\theta_c. \tag{10}$$

The dynamic contact angle used to generate the velocity dependencies $F = F(U)$ in Fig 4 has been obtained from the particle density profiles as is explained and illustrated in Supplementary Material. That is, the dynamic contact angle was defined at the interface between the bulk of the liquid and the liquid-gas, liquid-solid interfacial layers, exactly as it would have been defined in the macroscopic description.

The transition to the new regime with the precursor film present occurs at a universal branching point shown in Fig. 4, when the substrate velocity is at a critical value U_T, see Table 2.

Considering the behaviour of the dynamic contact angle θ_c in these cases at vanishing velocity, Fig 4, one can notice that the observed trend is not far from that, which might be expected from the Tanner's law $\theta_c^3 \propto Ca$ in the presence of a macroscopic precursor film, which is illustrated in Fig. 4 by experimental data.[39] Though in our case, there are several new features, which are solely conditioned by the distinctively microscopic character of the precursor film. This will be discussed later. Here, to understand the changes in the contact-line region invoked by the presence of the film, we first consider the processes taking place at the contact line region in its absence.

Dynamic processes at the contact-line region in the absence of the precursor film

In the previous studies,[8,17] we have already established that in the absence of the precursor film, in a range of velocities, the dynamic contact angle θ_c is solely conditioned by the nonlinear friction force acting on the first layer of liquid particles at the solid substrate, while the surface tensions of the liquid-gas and liquid-solid interfaces are expected to be at equilibrium.[15,16] The friction force is mostly distributed in a narrow region of several atomic diameters corresponding to the local contact line domain. There is, though, a tail of the force distribution of comparable to the capillary force strength resulting in non-local effects. This is illustrated in Figs. 5 and 6 in the case of complete wetting, when the substrate velocity is above the critical level $U > U_T$. In the current study, we substantially expand the parameter range to study the new regime.

The density distribution of the friction force δF (force per unit area) as a function of z has been obtained by sampling the force acting between liquid particles contained in a domain adjacent to the substrate of height $\Delta y = 3\,\sigma_{ff}$ and the solid wall particles. The liquid do-

main has been split in the z-direction into equal volume elements of the size $\Delta z = 1\,\sigma_{ff}$. The data have been averaged over the droplet depth in the x-direction and over the time interval $\Delta t = 10000\,\tau_0$.

The friction force distribution, which is shown in Fig. 5 (a), has two characteristic regions. In the first region, which begins at the tip of the precursor film, the distribution has a characteristic bell-shaped form, which is followed by a tail, where the friction force is practically uniform. One needs to note that the width of the bell-shaped region is definitely microscopic, and it is the tail of the distribution, where the friction force magnitude is still comparable to the capillary force strength, which can lead to nonlocal effects.

The tail of the friction force distribution in our simulations is due to the small and finite size of the system H, which corresponds well to the shear stress expected in the developed rectilinear flow between the solid substrates. Indeed, in the example shown in Fig. 5 (a), the shear stress in the tail region at $z > 20\,\sigma_{ff}$ at the solid substrate was found to be $\Theta_{yz} = -0.082 \pm 0.008\,f_0$, while the value of $\Theta_{yz} = -\frac{6\mu U}{H_{eff}} = -0.073\,f_0$ is expected assuming the Hagen-Poiseuille flow between the planes, where $H_{eff} = H - 2\Delta_S \approx 52\,\sigma_{ff}$ is the effective gap between the plates taking into account the size of the solid substrate $\Delta_S \approx 2.75\,\sigma_{ff}$.

As the system size increases, the value of the friction force in the tail region was observed to decrease at a given substrate velocity, as is expected in the rectilinear Hagen-Poiseuille flow conditions, and to eventually disappear in the macroscopic limit $H \to \infty$, see details in.[8] At the same time, the bell-shaped region in this length-scale limiting procedure was shown to be qualitatively invariant (subject to relatively minor quantitative changes), Fig. 5 (a), the dashed line, corresponding to the local force acting on the contact line.[8]

The transition to the bulk zone with the developed Hagen-Poiseuille flow can be also seen in the distribution of the surface velocity along the substrate (in the z-direction) measured in the boundary layer $\Delta y = 1.5\,\sigma_{ff}$ adjacent to the substrate, Fig. 5 (b).

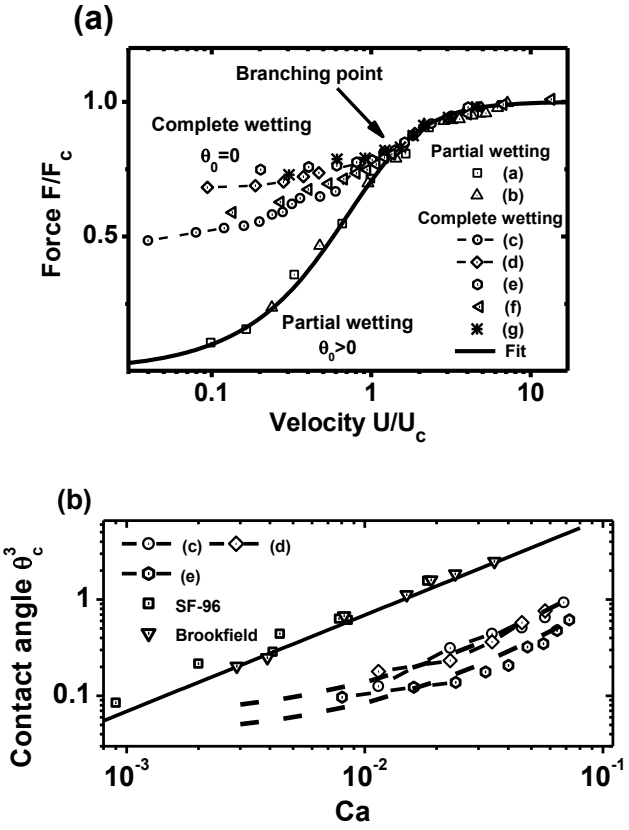

Figure 4: (a) Out-of-balance contact line force F/F_c as a function of velocity U/U_c at different conditions, Table 1. The solid line is the fit given by equation (11) (b) Dynamic contact angle θ_c^3 as a function of the capillary number $Ca = \frac{\mu U}{\gamma}$ at complete wetting. Symbols are for MDS, Tables 1 and 2, and the experiments with silicone fluids (Brookfield and SF–96).[39] The dashed lines are dependencies (13) and the solid line is the linear fit $\theta_c^3 \propto Ca$.

One can observe that in the bell-shaped region of the force distribution, the velocity at the solid surface substantially differs from the substrate velocity U, but quickly approaching it in the tail region. The velocity difference, which always exists irrespective of the system size H, is the main reason for the contact line friction force, which essentially modifies the force balance at the contact line.

Consider the force balance now in detail.

Force balance in the absence of the precursor film

Consider now the force balance given by equation (10). We first note that due to the use of long chain molecules there is practically no gas phase. Therefore, neglecting deformations of the solid substrate, the surface tension of the gas phase at the gas-solid interface is set to zero $\gamma_{GS} = 0$. Also, surface tensions defined on a macroscopic length scale in the tangential to the interfaces directions were found to be at equilibrium in accord with the previous analysis.[15,16]

The exact size, shape and location of the contact line zone on the microscopic length scale is the subject of a convention to some extent. In the macroscopic limit $H \to \infty$, the contact line zone is usually attributed to a point in the continuum, where at equilibrium the balance of surface tension forces is observed. In the study, we formally define a part of the contact line region, designated as an interface conflux, as the common place of two interfaces, an overlap of the interfacial layers with strong variations of density. This is indicated by a dashed box in Fig. 6.

If we were to ascribe the out-of-balance force F to the action of the friction force only $F = F_D$ and integrate the distribution of the tangential force δF along the z-direction (z_0 is chosen where the particle density is already negligible) $F_D = \int_{z_0}^{z_c} \delta F \, dz$, Fig. 6, one could see that the friction force alone should only balance the surface tension forces at $z_c = 14.3\,\sigma_{ff}$, that is on the length scale larger than that of the conflux region. The friction force acting on that length scale is insufficient to get the full balance, the disbalance being on the level of the surface tension, γ_0, Fig. 6.

At the same time, the velocity distributions clearly indicate that there is no strong force disbalance on the level suggested. This implies that the whole region in the vicinity of the dashed box in Fig. 6 is the subject of strong forces of non-hydrodynamic origin developed as a result of the prolonged action of the surface friction force. This is the direct evidence of the non-local character of the wetting line induced by the microscopic dimensions of the system.[14]

To verify this conclusion, we determined the component of the force acting on the dashed box, the force (per unit length in the x-direction) F_S acting on the surface element oriented perpendicular to the z-axis (a part of the right hand side of the dashed box at $z = -6\,\sigma_{ff}$) and of a variable side size Δy. It was found that the MDS data behave linearly with Δy as $F_S = A + B(\Delta y - \Delta y_0)$, $A = -2.3 \pm 0.1\,\gamma_0$, $B = 0.78 \pm 0.02 f_0$ and $\Delta y_0 = 0.44 \pm 0.1\,\sigma_{ff}$, as is expected in rectilinear fully developed viscous flows. Here, Δy_0 corresponds to the gap between the solid wall and the first layer of liquid molecules.

What was important was the magnitude of the force, which was clearly on the scale of the surface tension. The surface tension contribution (generated in the immediate vicinity of the substrate) can be extracted by taking the limit $\Delta y \to \Delta y_0$. One can observe that within the error band the value $A = -2.3 \pm 0.2\,\gamma_0$ matches $\gamma_{LS} = -2.3\,\gamma_0$ found independently, Table 1. Note, the force F_S will balance the liquid-gas surface tension $\gamma \cos\theta_c$ and the friction force acting on the bottom of the dashed box at $\Delta y \approx 2\,\sigma_{ff}$.

The total force balance on the dashed box in Fig. 6, which is certainly expected according to the distribution of the surface velocity v_S, Fig. 5 (b), is made of the surface tension forces and the extra force F generated by both the friction force $\int_{z_0}^{z_c} \delta F \, dz$ ($z_c = 6\,\sigma_{ff}$) and the non-hydrodynamic forces developed by the prolonged action of the friction force, all acting on the dashed box. Apparently, given the length scales involved, Figs. 5 and 6, the non-hydrodynamic force cannot be classified as

the capillary action.[40] In that sense, the example shown in Fig. 6 is interesting since it also illustrates the effect of non-locality due to the nano-scale size of the system. The prolonged mesoscopic tail of the tangential friction force distribution δF is able to influence the much smaller conflux part of the contact line region. The situation changes when the system size increases and becomes macroscopic.

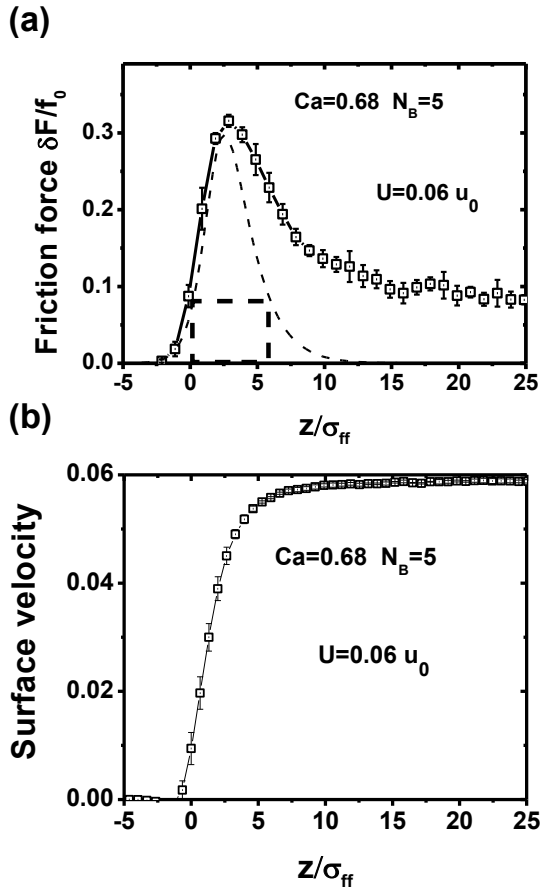

Figure 5: MDS in the complete wetting case, set (c) in Table 1, at $U = 0.06\,u_0$ and $\theta_c = 123°$: (a) Distribution of the tangential to the substrate friction force density δF as a function of z. The dashed line is the projected force distribution in the macroscopic limit $H \to \infty$ at the same system parameters. The conflux region is shown by a dashed box. (b) Distribution of the surface velocity v_S/u_0 in the boundary layer $\Delta y = 1.5\,\sigma_{ff}$ as a function of z.

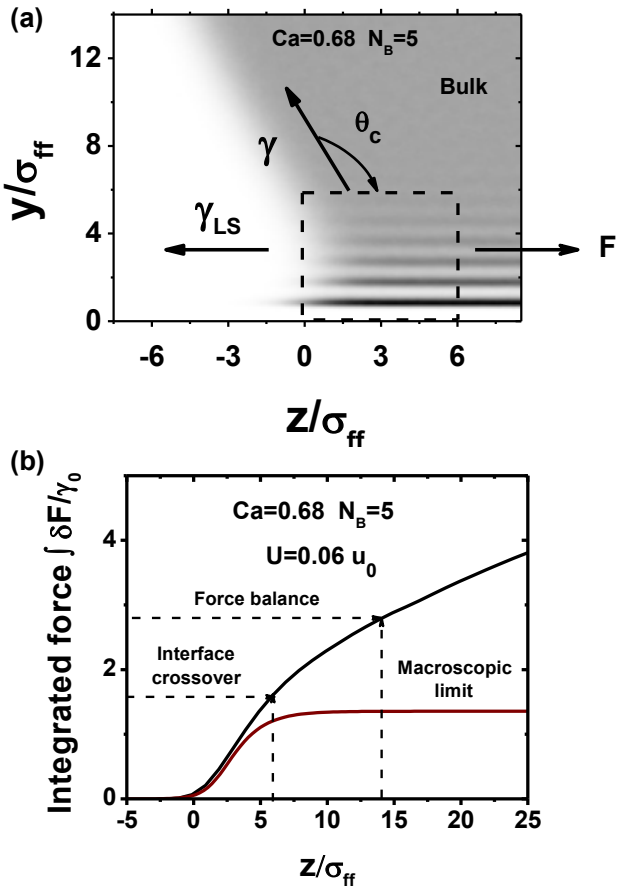

Figure 6: MDS, set (c) in Table 1, complete wetting at $U = 0.06\,u_0$ and $\theta_c = 123°$. (a) Force balance and the density distribution at the conflux region (dashed box). (b) The integrated friction force $F_D = \int_{z_0}^{z} \delta F\, d\xi$ as a function of z at $z_0 = -5\,\sigma_{ff}$. The upper solid line (black) is for the actual system, while the second, lower solid line (brown) is for its macroscopic limit. The dashed lines designate the contact line region end and the integration region to achieve the force balance $F_D + \gamma_{LS} + \gamma \cos\theta_c = 0$. Distances y and z are measured from the equimolar surface of the solid and the centre of the simulation box respectively.

Macroscopic limit in the absence of the precursor film

In the macroscopic limit, the friction force tail vanishes, and the force is localised. This is illustrated in Fig. 6, where the integral of the friction force distribution in the macroscopic limit $H \to \infty$ is shown as the brown line. Remarkably, the integral of the surface force distribution in the limit saturates within the conflux region, Fig. 6, though the force magnitude becomes slightly lower. Since the friction force would be localised within the conflux region in the macroscopic limit, all other non-hydrodynamic forces apart from the friction force are expected to vanish as well, so that the force balance is expected to be made, in this limit, of the surface tensions and the friction force only, as is manifested in the modified Young's equation (2). One can conclude that the definition of the conflux contact-line region as an intersection of the interfacial layers does make sense if the system size is essentially macroscopic. In this case, the contact line can be regarded as a local, one-dimensional object. On the other hand, if the system size is at the nanoscale, the effects of non-locality should manifest most clearly.

The modified force balance in turn affects the behaviour of the dynamic contact angle, which we consider next.

Dynamic contact angle

The velocity dependencies of the dynamic contact angle represented in terms of the out-of-balance force F at different parameters of the wetting system have been reduced to a single master curve, in the absence of the precursor film, by renormalizing the contact line velocity and the force, Fig. 4. This has been done by interpolating each dependence by a functional form

$$\frac{F}{F_c} = \frac{\frac{U}{U_c}}{\left(1 + \left(\frac{U}{U_c}\right)^2\right)^{\lambda}} \qquad (11)$$

with two adjusting parameters F_c and U_c, and a fixed value of $\lambda = 1/2$. The functional form (11) was inspired by the MDS of the liquid slip behaviour,[41–43] where the liquid-solid friction, also the mechanism of the dynamic contact angle generation,[8] was directly measured. The choice of $\lambda = 1/2$ in the fitting function is dictated by the observed saturation of the friction force (F tends to a constant value) in the high velocity limit. The fact that all the force-velocity dependencies $F = F(U)$ after the renormalisation confine to a single master curve implies that the mechanism of the dynamic contact angle generation due to the friction force is indeed universal, at least in the systems in hands, and all the friction force parameters are changing in a congruent way during variations of the surface interaction potential, liquid properties and the temperature in the system.

The velocity dependencies in the complete wetting cases followed the trend (11) initially, in the high velocity region, but deviated from the master curve at a universal branching point when the velocity fell below a critical value U_T, Table 2. While the values of the critical velocity U_T and the corresponding friction force F_T strongly depend on the system parameters, remarkably, the normalised quantities $U_T/U_c \approx 1.6$ and $F_T/F_c \approx 0.83$ are practically invariant, Table 2. This implies that initially before entering the diffusive regime, the precursor film has a certain velocity only conditioned by a single parameter U_c, which in turn is defined by the system parameters contributions to the friction force.

At the critical point, the velocity dependencies deviated from the master curve and instead developed into a plateau. The appearance of the plateau coincided with the onset of the precursor film, so that now we will turn our attention to this special regime of dynamic wetting.

Dynamic processes and the force balance at the contact-line region in the presence of the precursor film

Consider the dynamics in the plateau regime in more detail. The distribution of the friction force δF, the surface density ρ_S and the tangential surface velocity v_S along the substrate

are shown in Fig. 7. The surface variables have been obtained by averaging over the boundary layer $\Delta y = 1.5\,\sigma_{ff}$ adjacent to the substrate, over the droplet depth (in the x-direction) and over the time interval $\Delta t = 10000\,\tau_0$. The case shown in the picture corresponds to a sufficiently developed tail at $U = 0.009\,u_0$, see distribution of the particle density in Fig. 8. The part of the contact line zone defined again as the overlapping region of the two interfaces is shown by a dashed box.

As one can see, in contrast to the case in the absence of the precursor, both distributions, $\rho_S(z)$ and $v_S(z)$, extend on much larger length-scale (tens of σ_{ff} or about 10 nm in dimensional units) even at the onset of the precursor regime. They demonstrate strong variations within the tail region shown in Fig. 8, while they appear to be almost at equilibrium when approaching the contact line zone defined by the overlap.

The surface velocity distribution has three distinctive regions. Initially, at the precursor film tip, one can clearly observe fluctuations of the contact line position. The particles at the tip of the film are seen to be moving away. This is the transient feature, as zero average velocity in the steady state is expected. It can only be observed due to the finite observation time and the very small number of particles at the tip of the film.

Further down the substrate, the velocity distribution conforms to the rolling motion, when the surface velocity is attaining the velocity of the substrate, while the average velocity in the film is zero. Away from the contact line zone, the velocity attains a constant value, which is close to the substrate velocity with a small slip component present, Fig. 7 (c).

The result of the velocity and the density distributions is the friction forces acting on the first layer of liquid molecules, Fig. 7 (a). As one can see, the friction force vanishes at the conflux (the dashed box), so that the energy dissipation takes place mostly in the precursor film region. This also implies that strong non-hydrodynamic forces from the exterior of the contact line region (apart from the friction force itself) can be disregarded in the force balance.

The force balance in the presence of a precursor

As it appears, the force balance in this case is quite different from that, which would be expected without the film present. The surface density distribution directly implies that the liquid-solid surface tension (neglecting deformations of the solid) is continuous through the contact line zone, which was confirmed by independent measurements. So that, the only forces acting on the dashed box are from the liquid-gas interface $\gamma\cos\theta_c$, the friction force F_D and the force exerted by the running away liquid film F_p, Figs. 7 (a) and 8.

As a numerical example, consider a particular case, set (c) in Table 1 at $U = 0.009\,u_0$ and $\theta_c = 68.7°$. The force balance

$$F_D + F_p + \gamma\cos\theta_c = 0 \qquad (12)$$

directly implies that at $F_D = \int_{z_1=-23\,\sigma_{ff}}^{z_2=-17\,\sigma_{ff}} \delta F\,dz = 0.5 \pm 0.1\,\gamma_0$, $F_p = -0.85 \pm 0.1\,\gamma_0$. As one can see, the force from the film is close to the value expected from the surface tension of the free surface $\gamma = 0.92\,\gamma_0$, despite the film being microscopic. This is due to the behaviour of the interface potential $g(h_f)$ or equivalently the Derjaguin pressure $\Pi(h_f) = -\frac{dg}{dh_f}$ upon decreasing the film thickness h_f.[44] Both quantities are used to quantify the interaction between the two interfaces, that is deviation of the interfacial free energy from the sum of two independent components γ and γ_{LS}. The interface potential $q(h_f)$, as it has been observed in MDS,[44] is quickly vanishing when $h_f > 2\,\sigma_{ff}$, exactly as it happens at the contact line region where the film thickness is already $h_f \approx 2.5\,\sigma_{ff}$.

One may expect that the friction force acting on the tail, $F = \int_{z_1=-40\,\sigma_{ff}}^{z_2=-23\,\sigma_{ff}} \delta F\,dz$, is proportional on average to the length of the film and the substrate velocity (the friction force in the linear regime is proportional to the velocity[41–43]), that is $F \propto UL_p$. But, as we have established $L_p \propto U^{-1}$. So that on average, approximately F is supposed to be independent of the velocity U, which has been indeed ob-

served in the MDS. Therefore, the force exerted by the precursor film on the conflux F_p could be regarded as an invariant, so that the only component contributing to the contact angle variations with U through the force balance is the friction force F_D.

To test the conjecture, we take into account that the friction force F_D is expected to behave linearly with the capillary number in this regime

$$F_D = \alpha\, Ca$$

where α is chosen such that at a reference point ($\alpha = 5\,\gamma_0$ at $U = 0.009\,u_0$, $Ca = 0.1$ in our example), the force F_D is equal to the integral of the force distribution over the conflux region, Fig. 8, ($F_D = 0.5\,\gamma_0$ and $F_p = 0.85\,\gamma_0$ at $Ca = 0.1$ in our example). Then

$$\cos\theta_c = \frac{F_p - \alpha Ca}{\gamma}. \tag{13}$$

A comparison between (13) and the contact angle dependencies observed in MDS is shown in Fig. 4 (b) demonstrating quite good agreement.

One can observe, that the new trend is in some contrast to the Tanner's law $\theta_c^3 \propto Ca$,[45] since the contact angle tends to a plateau at a finite value instead of tending to zero. This effect is solely due to the microscopic dimensions of the precursor film at the foot of the liquid volume.

Shall the film thickness at the liquid volume foot become larger, $F_p = \gamma$ and the contact angle will tend to zero, but with slightly different asymptotic behaviour. Neglecting the effects of the disjoining pressure, the force balance can be simplified to

$$F_D + \gamma(\cos\theta_c - 1) = 0. \tag{14}$$

That is, the variations of the contact angle θ_c are only driven by the friction force, and the other substrate parameters are contributing in the variations only through this quantity.

The force balance (14) implies $\theta_c^3 \propto Ca^\lambda$ at $\lambda = 1.5$ rather than $\lambda = 1$. We note that the Tanner's law asymptotic behaviour at $\lambda = 1$ is only expected in truly macroscopic conditions at the inflection point of the free surface profile as a result of the thin film approximation. For example, the experimental data with silicone oils,[39] shown for comparison in Fig. 4 (b), clearly demonstrate the Tanner's law trend $\theta_c^3 \propto Ca$. It is very likely that the real substrate used in the experiments was not atomically smooth negotiating the film thickness to be on a larger scale than that of the atomic length scale. On the other hand, the scaling experimentally observed for 100 nm precursor films was somewhat in between at $\lambda = 1.2$,[46] so that the MDS scaling is not in that sense extraordinary. Therefore, one can expect that the specific new trends from the microscopic advancing precursor film should be pronounced and dominant at the nanoscale, especially in the case of such materials as graphene with the sub-atomically smooth surface.

The observed characteristic behaviour of the dynamic contact angle in the presence of a precursor film has direct implications on the dynamics of drop spreading. If we consider spreading droplets in the spherical approximation with the base radius R and small contact angles ($\tan\theta_c \approx \theta_c$), then by conservation of volume $\theta_c R^3 = const$. If we also assume a power law time dependence of the variables, as is regularly observed in experiments,[47,48] that is $R(t) \propto t^\beta$, then the scaling $\theta_c^3 \propto Ca^\lambda$ ($Ca \propto dR/dt$) suggests

$$\beta = \frac{\lambda}{9+\lambda}.$$

As a result, at $\lambda = 1$, one can expect

$$R \propto t^{1/10}, \quad \theta_c \propto t^{-3/10}, \tag{15}$$

while at $\lambda = 3/2$, the spreading should proceed at a rather different exponent

$$R \propto t^{1/7}, \quad \theta_c \propto t^{-3/7}. \tag{16}$$

In that respect, it is interesting to draw parallels with a set of experiments conducted at nearly complete wetting conditions.

Multiple time scales in drop spreading experiments and contact line non-locality

Another experimental evidence of the anomalous scaling with $\lambda = 1.5$ comes from the observation of multiple time scales during the spreading of organosilicon liquid drops on silicon wafers, though in the almost complete wetting case (very small equilibrium contact angles $\theta_0 \approx 0.1^\circ$) during an intermediate phase of the drop dynamics.[47,48] Consider those results in a bit more detail.

There were two kinds of dynamic behaviour observed. After some initial (relatively short) phase of spreading, the drop radius R and the contact angle θ_c followed the scaling suggested by (16). This dynamics continued until some characteristic time, when the time evolution turned into the scaling expected from the Tanner's solution, that is (15).

In the study analysis, the two regimes of spreading were attributed to the dissipation in two different channels: friction against the substrate and hydrodynamic effects.[47,48] On the other hand, while this was not directly observed in the experiments, one may wonder, given relatively low lateral experimental resolution ($\approx 0.1\,\mu$m) if the contact line structure at the very small contact angles was similar to that with a short (a few nanometers) precursor film formed in front of the spreading volume. This could be the direct experimental evidence that the initially molecularly thin precursor films were developed into wider mesoscopic structures influencing the force balance, the contact angle dynamics and hence the rate of the drop spreading.

Conclusions

The dynamic wetting phenomena at the onset of a precursor film have been studied from the first principles of MDS using a combination of the well-defined steady states and macroscopic observables. The main result of the study is the detailed microscopic structure of the contact line region (the surface distributions of density, velocity and the friction force) at the onset of the precursor film regime coupled with macroscopic observables, such as the dynamic contact angle, Figs. 7 and 8, and with the force balance (14).

It has been found that in contrast to the simple (no film present) advancing motion, Figs. 5 and 6, the contact-line region in this regime becomes essentially non-local with a somewhat non-trivial structure enabling an interplay between the surface distributions of density and velocity, which manifested on macroscopic length scales, Figs. 7 and 8. Again in contrast to the simple advancing motion, the non-local effects at the contact line in this case are insensitive to the system size, and will not disappear in the macroscopic limit.

This outcome provides a universal conceptual basis to analyse dynamic wetting regimes in the capillary flows involving precursors. The results are especially important in the parameter range when the precursor film just starts developing considering rather limited experimental resolution in the parallel to the flow direction, which could make it difficult to detect such a feature.[38,46]

There are several particular results, which are summarised below.

- It has been found, that the generic force balance represented by the modified Young's law,[8] relation (2), has changed, relation (14) due to the presence of the precursor film.

- It has been established, that the non-locality of the contact line region and the associated phenomena can not be in principle captured by a localised approach. That is, for example, the tip of the moving precursor film, which can be described by the molecular kinetic theory,[9–11] has little influence on the force balance in the region where the contact angle is generated in this case. Also note, that the effects of the surface deformations[24] will mostly manifest at the precursor film tip, while the force acting on the solid surface at the conflux region is expected to be rather weak.

- At the same time, the analysis and simulations have demonstrated that the force balance, which manifests macroscopically through the dynamic contact angle, can still be formulated using the local conflux part (intersection of the surface layers) of the contact-line region, Fig. 8, as is expected in macroscopic formulations. These results are conceptually fundamental and can be used in modelling methodologies, practical applications and interpretation of experimental data.

- It has been established that the microscopic character of the moving ahead precursor film results in non-trivial contact-angle behaviour at vanishing velocities in some contrast to the Tanner's law[45] observed for truly macroscopic film structures. This behaviour seems to be in accord with the experimental observations[46] and has striking similarities with that found in spreading regimes of droplets, when multiple time scales were observed.[47,48] The non-trivial character of the contact angle-velocity dependence has interesting repercussions in relation to the dynamics of drops spreading, which may be used to identify this spreading regime (precursor present) by measuring macroscopic, apparent contact angle behaviour.

- It was found that the transition to the wetting regime with a precursor film present occurs in a non-dimensional parameter space at a universal branching point, Fig. 4, which can be used in interpretation of experimental data and in predictive analysis.

As the notion of the contact line is conceptually fundamental to the capillary science,[26] the developed framework and the outcomes are rather universal and applicable to a wide range of capillary flows to understand and to interpret experimental data, and to predict the effects of dynamic wetting in practical applications. The outcomes are especially pertinent to the analysis of capillary phenomena taking place at nanoscale in confined geometries, where the non-local effects should lead to rather non-trivial interplays, which would be difficult to interpret otherwise.

In future, this would be interesting to extend the analysis to the larger precursor length scales, so that to be able to observe a transition to the Tanner's law regime, and to more complex molecular systems to understand the scope of the results found in this study.

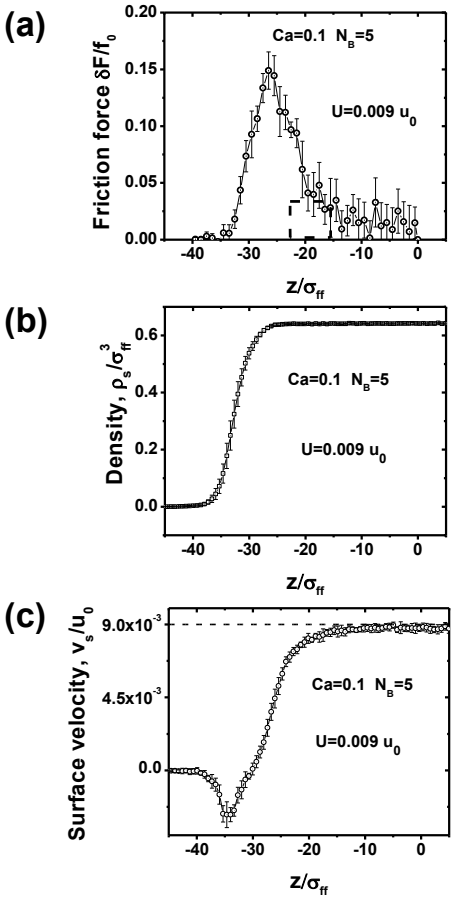

Figure 7: MDS, set (c) in Table 1, complete wetting at $U = 0.009\,u_0$ and $\theta_c = 68.7°$. (a) Tangential component of the friction force δF, (b) surface density ρ_S and (c) surface velocity v_S as functions of z. The dashed box designates the contact line region, with similar dimensions as in Fig. 6. The surface variables have been obtained in the boundary layer $\Delta y = 1.5\,\sigma_{ff}$ at the solid wall.

References

(1) Young, T. An essay on the cohesion of fluids *Phil. Trans. R. Soc. London* **1805**, 95,

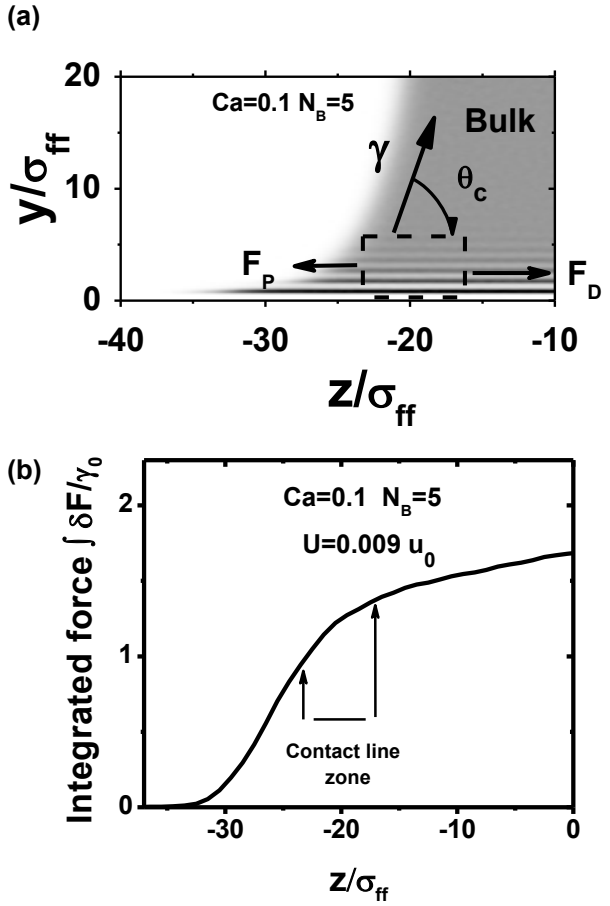

Figure 8: MDS, set (c) Table 1, complete wetting at $U = 0.009\,u_0$ and $\theta_c = 68.7°$. (a) Force balance and the density distribution at the contact line region designated by the dashed box. (b) The integral of the tangential component of the friction force $\int_{z_0}^{z} \delta F\, d\xi$ as a function of z. Distances y and z are measured from the equimolar surface of the solid and the centre of the simulation box respectively.

65–87

(2) Leger, L. and Joanny, J.F. Liquid spreading *Rep. Prog. Phys.* **1992**, 55, 431–486

(3) Roura, P. and Fort, J. Local thermodynamic derivation of Young's equation *J. Colloid Interface Sci.* **2004**, 272, 420–429

(4) Finn, R. The contact angle in capillarity *Phys. Fluids* **2006**, 18, 047102

(5) Ingebrigtsen, T. and Toxvaerd, S. Contact Angles of Lennard-Jones Liquids and Droplets on Planar Surfaces *J. Phys. Chem. C* **2007**, 111, 8518–8523

(6) Snoeijer, J.H. and Andreotti, B. A microscopic view on contact angle selection *Phys. Fluids* **2008**, 20, 057101

(7) Seveno, D.; Blake, T.D. and De Coninck, J. Young's Equation at the Nanoscale *Phys. Rev. Lett.* **2013**, 111, 096101

(8) Lukyanov, A.V. and Likhtman, A.E. Dynamic Contact Angle at the Nanoscale: A Unified View *ACS Nano* **2016**, 10, 6045–6053

(9) Blake, T.D. and Haynes, J.M. Kinetics of Liquid/Liquid Displacement. *J. Colloid Interface Sci.* **1969**, 30, 421–423

(10) Blake, T.D. The physics of moving wetting lines *J. Colloid Interface Sci.* **2006**, 299, 1–13

(11) Bertrand, E.; Blake, T.D. and De Coninck, J. Influence of solid-liquid interactions on dynamic wetting: a molecular dynamics study *J. Phys.: Condens. Matter* **2009**, 21, 464124

(12) Darhuber, A.A. and Troian, S.M. Principles of microfluidic actuation by modulation of surface stresses *Annu. Rev. Fluid Mech.* **2005**, 37, 425–455

(13) Blake, T.D.; Bracke, M. and Shikhmurzaev, Y.D. Experimental evidence of nonlocal hydrodynamic influence on the dynamic contact angle *Phys. Fluids* **1999**, 11, 1995–2007

(14) Blake, T.D.; Fernandez-Toledano, J.C.; Doyen, G. and De Coninck, J. Forced wetting and hydrodynamic assist *Phys. Fluids* **2015**, 27, 112101

(15) Lukyanov, A.V.; Likhtman, A.E. Relaxation of Surface Tension in the Free-Surface Boundary Layer of Simple Lennard-Jones Liquids. *J. Chem. Phys.* **2013**, 138, 034712

(16) Lukyanov, A.V.; Likhtman, A.E. Relaxation of Surface Tension in the Liquid-Solid Interfaces of Lennard-Jones Liquids. *Langmuir* **2013**, 29, 13996–14000

(17) Lukyanov, A.V.; Pryer, T. Hydrodynamics of moving contact lines: Macroscopic versus microscopic. *Langmuir* **2017**, 33, 8582–8590

(18) Webb, E.B.; Grest, G.S. and Heine, D.R. Precursor Film Controlled Wetting of Pb on Cu. *Phys. Rev. Lett.* **2003**, 91, 236102

(19) Nosonovsky, M. Model for solid-liquid and solid-solid friction of rough surfaces with adhesion hysteresis *J. Chem. Phys.* **2007**, 126, 224701

(20) Bormashenko, E.; Bormashenko, Y.; Whyman, G.; Pogreb, R.; Musin, A.; Jager, R. and Barkay, Z. Contact angle hysteresis on polymer substrates established with various experimental techniques, its interpretation, and quantitative characterization. *Langmuir* **2008**, 24, 4020–4025

(21) Pericet-Cámara, R.; Best, A.; Butt, H.J. and Bonaccurso, E. Effect of Capillary Pressure and Surface Tension on the Deformation of Elastic Surfaces by Sessile Liquid Microdrops: An Experimental Investigation *Langmuir* **2008**, 24, 10565–10568

(22) Leh, A.; N'guessan, H.E.; Fan, J.; Bahadur, P.; Tadmor, R. and Zhao, Y. On the Role of the Three-Phase Contact Line in Surface Deformation *Langmuir* **2012**, 28, 15795–15801

(23) Weijs, J.H.; Andreotti, B.; Snoeijer, J.H. Elasto-Capillarity at the Nanoscale: on the Coupling Between Elasticity and Surface Energy in Soft Solids. *Soft Matter* **2013**, 9, 8494–8503

(24) Butt, H.J.; Berger, R.; Steffen, W.; Vollmer, D. and Weber, S.A.L. Adaptive Wetting–Adaptation in Wetting *Langmuir* **2018**, 34, 11292–11304

(25) Tadmor, R. Open Problems in Wetting Phenomena: Pinning Retention Forces *Langmuir* **2021**, 37, 6357–6372

(26) de Gennes, P.G. Wetting: statics and dynamics. *Rev. Mod. Phys.* 57, 827–863 **1985**,

(27) Cazabat, A.M. How does a droplet spread? *Contemp. Phys.* 28, 347–364 **1987**,

(28) Heslot, F.; Fraysse, N. and Cazabat, A.M. Molecular layering in the spreading of wetting liquid drops *Nature* 338, 640–642 **1989**,

(29) Beaglehole, D. Profiles of the Precursor of Spreading Drops of Siloxane Oil on Glass, Fused Silica, and Mica *J. Phys. Chem.* 93, 893–899 **1989**,

(30) Heslot, F.; Cazabat, A.M. and Fraysse, N. Diffusion-controlled wetting films *J. Phys. Condens. Matter* 1, 5793–5798 **1989**,

(31) Cazabat, A.M.; Fraysse, N.; Heslot, F. and Carles, P. Spreading at the Microscopic Scale *J. Phys. Chem.* 94, 7581–7585 **1990**,

(32) Cazabat, A.M.; Fraysse, N.; Heslot, F.; Levinson, P.; Marsh, J.; Tiberg, F. and Valignat, M.P. Pancakes *Adv. Colloid Interface Sci.* 48, 1–17 **1994**,

(33) Min, B.G.; Choi, J.W.; Brown, H.R.; Yoon, D.Y.; ÓConnor, T.M. and Jhon, M.S. Spreading characteristics of thin liquid films of perfluoropolyalkylethers on

solid surfaces. Effects of chain-end functionality and humidity *Tribol. Lett.* 1, 225–232 **1995**,

(34) Ala-Nissila, T.; Herminghaus, S.; Hjelt, T. and Leiderer, P. Diffusive Spreading of Chainlike Molecules on Surfaces *Phys. Rev. Lett.* 76, 4003–4006 **1996**,

(35) Voué, M.; Valignat, M.P.; Oshanin, G. ; Cazabat, A.M. and De Coninck, J. Dynamics of Spreading of Liquid Microdroplets on Substrates of Increasing Surface Energies *Langmuir* 14, 5951–5958 **1998**,

(36) Voué, M.; Semal, S. and De Coninck, J. Dynamics of Spreading on Heterogeneous Substrates in a Complete Wetting Regime *Langmuir* 15, 7855–7862 **1999**,

(37) Chibbaro, S.; Biferale, L.; Diotallevi, F.; Succi, S.; Binder, K.; Dimitrov, D.; Milchev, A.; Girardo, S. and Pisignano, D. Evidence of thin-film precursors formation in hydrokinetic and atomistic simulations of nano-channel capillary filling *EPL* 84, 44003 **2008**,

(38) Popescu, M.N.; Oshanin, G.; Dietrich, S. and Cazabat, A.M. Precursor films in wetting phenomena *J. Phys. Cond. Matter* 24, 243102 **2012**,

(39) Hoffman, R.L. A study of the advancing interface. I. Interface shape in liquid—gas systems *J. Colloid Interface Sci.* 50, 228–241 **1975**,

(40) Rowlinson, J.S. and Widom, B. *Molecular Theory of Capillarity.* (Dover Publications, 2002).

(41) Thompson, P.A.; Troian, S.M. A general boundary condition for liquid flow at solid surfaces *Nature* **1997**, 389, 360–362

(42) Priezjev, N.V.; Troian, S.M. Molecular Origin and Dynamic Behavior of Slip in Sheared Polymer Films. *Phys. Rev. Lett.* **2004**, 92, 018302

(43) Priezjev, N.V. Relationship Between Induced Fluid Structure and Boundary Slip in Nanoscale Polymer Films. *Phys. Rev. E* **2010**, 82, 051603

(44) Tretyakov, N.; Müller, M.; Todorova, D. and Thiele, U. Parameter passing between molecular dynamics and continuum models for droplets on solid substrates: The static case. *J. Chem. Phys.* 138, 064905 **2013**,

(45) Tanner, L.H. The spreading of silicone oil drops on horizontal surfaces *J. Phys. D: Appl. Phys.* 12, 1473 **1979**,

(46) Kavehpour, H.P.; Ovryn, B. and McKinley, G.H. Microscopic and Macroscopic Structure of the Precursor Layer in Spreading Viscous Drops. *Phys. Rev. Lett.* 91, 196104 **2003**,

(47) De Ruijter, M.J.; De Coninck, J. and Oshanin, G. Droplet Spreading: Partial Wetting Regime Revisited *Langmuir* 15, 2209–2216 **1999**,

(48) De Ruijter, M.J.; Charlot, M.; Voué, M. and De Coninck, J. Experimental Evidence of Several Time Scales in Drop Spreading *Langmuir* 16, 2363–2368 **2000**,